

Sustainable Food Technology

Accepted Manuscript

This article can be cited before page numbers have been issued, to do this please use: N. Asaithambi and A. Ubeyitogullari, *Sustainable Food Technol.*, 2025, DOI: 10.1039/D6FB00025H.



This is an Accepted Manuscript, which has been through the Royal Society of Chemistry peer review process and has been accepted for publication.

Accepted Manuscripts are published online shortly after acceptance, before technical editing, formatting and proof reading. Using this free service, authors can make their results available to the community, in citable form, before we publish the edited article. We will replace this Accepted Manuscript with the edited and formatted Advance Article as soon as it is available.

You can find more information about Accepted Manuscripts in the [Information for Authors](#).

Please note that technical editing may introduce minor changes to the text and/or graphics, which may alter content. The journal's standard [Terms & Conditions](#) and the [Ethical guidelines](#) still apply. In no event shall the Royal Society of Chemistry be held responsible for any errors or omissions in this Accepted Manuscript or any consequences arising from the use of any information it contains.

Sustainability Spotlight

This work addresses the global challenge of fruit and vegetable waste by valorizing the whole food residues into high-value, functional aerogels without extraction or chemical-intensive processes. Using SC-CO₂ as a sustainable green technique for drying, we process fruits and vegetable waste materials such as banana peels, broccoli stems, cabbage leaves, imperfect carrots, and orange peels into lightweight, highly porous aerogels for various applications, including wastewater treatment. This approach supports circular economy principles by reducing food waste, minimizing resource use, and creating sustainable materials for water purification and filtration. Moreover, the study contributes to UN Sustainable Development Goals (SDG) of responsible production and consumption as well as safe water, sanitization, and hygiene by highlighting both waste reduction and sustainable water treatment solutions.



1 **Generating high-value porous materials from fruit and vegetable waste**

2

3

4

5 Niveditha Asaithambi^a, and Ali Ubeyitogullari^{a,b*}

6 ^a Department of Food Science, University of Arkansas, Fayetteville, AR 72704, USA

7 ^b Department of Biological and Agricultural Engineering, University of Arkansas, Fayetteville,
8 AR 72701, USA

9

10

11

12

13

14 *Corresponding author

15 Ali Ubeyitogullari

16 Email: uali@uark.edu

17 Tel: +1 (479)-575-3183

18 2650 N. Young Ave., Room N205

19 Fayetteville, AR 72704



20 Abstract

21 Fruit and vegetable waste is a global concern due to its significant environmental impact,
22 economic loss, and implications for food security. In this study, fruit and vegetable waste was
23 used as whole materials, avoiding extraction, to produce aerogels via supercritical carbon dioxide
24 (SC-CO₂) drying for applications of dye removal. Aerogels were produced from banana peel
25 (BPA), broccoli stem (BSA), cabbage leaves (CLA), imperfect carrot (ICA), and orange peel
26 (OPA). The resulting aerogels exhibited low density (<1 g/cm³), high porosity (>93%), and high
27 surface areas (12-172 m²/g), with OPA showing the highest value at 172 m²/g. The CLA samples
28 had the highest pore size (29 nm), contributing to their highest water absorption capacity of 95%.
29 SEM images showed a promising porous structure and highlighted the fibrillar structure in OPA
30 samples. The average methylene blue adsorption capacity was ~84%, except for OPA samples
31 (53%). The methylene blue adsorption was driven by electrostatic interactions, which highly
32 correlated with the pseudo-first order kinetic model ($R^2 > 0.98$). Overall, this study demonstrates
33 that whole fruit and vegetable waste can be effectively converted into lightweight, highly porous
34 aerogels with potential applications in biomedical and food fields, purification and filtration
35 systems, and other functional materials sectors.

36 **Keywords:** Fruit, vegetable, waste, supercritical carbon dioxide, upcycling, aerogel, surface
37 area, dye adsorption.

38 Sustainability Spotlight

39 This work addresses the global challenge of fruit and vegetable waste by valorizing the
40 whole food residues into high-value, functional aerogels without extraction or chemical-intensive
41 processes. Using SC-CO₂ as a sustainable green technique for drying, we process fruits and
42 vegetable waste materials such as banana peels, broccoli stems, cabbage leaves, imperfect



43 carrots, and orange peels into lightweight, highly porous aerogels for various applications,
44 including wastewater treatment. This approach supports circular economy principles by reducing
45 food waste, minimizing resource use, and creating sustainable materials for water purification
46 and filtration. Moreover, the study contributes to the UN Sustainable Development Goals (SDG)
47 of responsible production and consumption as well as safe water, sanitization, and hygiene by
48 highlighting both waste reduction and sustainable water treatment solutions.



49 1. Introduction

50 Food waste represents a major global challenge in the food industry. Developing
51 sustainable strategies to valorize these waste materials is crucial for promoting circular economy
52 practices. According to the Food and Agriculture Organization of the United Nations (FAO),
53 approximately 1.3 billion tons of food are wasted each year globally, resulting in an estimated
54 monetary loss of about USD 936 billion, excluding the significant environmental and social costs
55 borne by society as a whole ¹. The United Nations Sustainable Development Goal (SDG) Target
56 12.3 aims to reduce the global food loss and waste by 50% by 2030, through prevention,
57 reduction, recycling, and reuse of food resources. Achieving this task requires the development
58 of innovative technologies and processing strategies to support regenerative practices, conserve
59 resources, and minimize greenhouse gas emissions, which have become a crucial focus in recent
60 years ².

61 Among total food waste, approximately 16% is contributed by fruits and vegetables,
62 which also account for about 6% of global greenhouse gas emissions ³. The wide diversity of
63 horticultural products makes them unique among food resources, offering numerous possibilities
64 for value addition through innovative processing and utilization of their natural components.
65 Most studies on fruit waste utilization focus on the recovery of bioactive compounds that exhibit
66 antioxidant, antimicrobial, or health-promoting properties with potential applications in
67 pharmaceuticals, packaging films, and functional food development ^{4, 5}. However, the efficiency
68 of bioactive compound extraction depends on several critical factors, including the source
69 material, extraction technology, and processing methods, and still leaves behind a large fraction
70 of food waste materials ⁶. Therefore, an alternative strategy for food waste valorization involves



71 converting it into high-value aerogels through green, sustainable, and economically viable
72 methods ².

73 Another major environmental concern is the organic dyes used in the paper and textile
74 industries to enhance their aesthetic appeal and gloss, which are a major source of water
75 pollution ⁷. Their presence in wastewater poses serious environmental and health risks, making
76 their removal a critical global concern. Although several remediation strategies have been
77 developed, the elimination of dyes remains challenging due to their complex molecular
78 structures, large size, and high chemical stability, particularly in the case of dyes such as
79 methylene blue ^{8,9}.

80 Aerogels are porous materials characterized by high surface area (>100 m²/g), low
81 density, excellent absorption capacity, and low thermal conductivity ¹⁰. They are typically
82 produced from organic or synthetic polymers by first forming a gel, followed by solvent
83 exchange to remove the water, and finally drying via SC-CO₂. This results in a solid network of
84 interconnected nanoparticles or polymer chains filled mostly with air ¹¹. Recent research has
85 focused more on developing bio-based aerogels that are environmentally friendly and
86 economically viable. Some of the common biopolymers used in aerogel preparation include
87 polysaccharides (e.g., starch, pectin, alginate, chitosan, chitin, cellulose, and its derivatives) and,
88 in some cases, proteins ¹²⁻¹⁴. Recently, Possari, *et al.* ¹⁵ utilized biomass from the orange juice
89 industry to produce biobased aerogels using citric acid hydrolysis. These biopolymer-derived
90 aerogels, which rely on processing and extraction-based approaches, have found numerous
91 applications, including use as an insulating material, adsorbents, biomedical applications, and
92 active food packaging ^{12, 16}.



93 Although aerogels have been successfully produced from natural biopolymers, the
94 extraction process is often time-consuming and labor-intensive. Moreover, these aerogels often
95 involve the use of hazardous chemicals during processing, which can pose environmental and
96 health risks and limit their overall sustainability ^{17,18,19}. Therefore, developing simpler and more
97 innovative methods for aerogel production is essential. In this study, for the first time, we report
98 the direct conversion of fruit and vegetable waste into aerogels to understand their structural and
99 functional characteristics for potential future applications. Previously, Gibowsky, *et al.* ²
100 utilized fresh fruits and vegetable tissues that were pulp removed or shredded, solvent-exchanged
101 using ethanol, and then dried using SC-CO₂, to form porous aerogels. However, the biowaste as
102 a whole was not utilized in previous studies. Therefore, aerogels derived from food waste not
103 only address waste management concerns but also provide an eco-friendly and versatile platform
104 for the efficient adsorption and removal of organic dyes from wastewater. Here, we employ SC-
105 CO₂ technology, a widely used, green, cost-effective, and unique technique that is Generally
106 Recognized as Safe (GRAS) to produce aerogels. The technology has been advantageous in
107 producing aerogels with a high surface area. In our previous study ¹⁴, we found that the SC-CO₂-
108 dried starch beads showed a significantly higher surface area (175 m²/g) than the freeze-dried
109 ones (<1 m²/g).

110 Therefore, in this study, we investigated the direct formation of food waste-derived
111 aerogels from various fruit and vegetable sources (i.e., banana peel, broccoli stem, cabbage
112 leaves, imperfect carrot, and orange peel) using SC-CO₂ drying. These fruit and vegetable waste
113 samples were selected due to their generation in large quantities as well as their potential to form
114 a porous structure ^{20, 21}. The samples were characterized for their physicochemical and structural



115 properties for their potential applications in the removal of dyes to prevent environmental
116 pollution.

117 **2. Experimental Section**

118 **2.1. Materials**

119 The fruit and vegetable samples, including navel orange peels, imperfect carrots, broccoli
120 stems, cabbage leaves, and banana peels, were obtained from a local store/farm. The ethanol
121 utilized for solvent exchange was purchased from Decan Labs, Inc. (Koptec, Pure Ethanol 200
122 Proof, PA, USA). The liquid CO₂ (99.99% purity) for the SC-CO₂ system was procured from
123 Airgas, Inc. (AR, USA).

124 **2.2 Aerogel formation**

125 For aerogel preparation, all materials were cut into small pieces (~1-5 cm) and weighed
126 before the solvent exchange process. Next, the prepared samples were solvent exchanged by
127 sequential immersion in ethanol/water solutions of 30%, 50%, 70% and 100% ethanol, each for 1
128 h, followed by immersion in 100% ethanol for 24 h. Later, the samples were dried using a lab-
129 scale SC-CO₂ system (SFT-120, Supercritical Fluid Technologies Inc., DE, USA) at 10 MPa and
130 40 °C for 4 h, with a CO₂ flow rate of 1.0 L/min (measured under ambient conditions of 23 °C
131 and 0.1 MPa)¹³. The resulting aerogels were then collected and stored at room temperature (23
132 °C) in airtight containers until further analysis.

133 **2.3. Moisture content**

134 The moisture contents of fresh fruit and vegetable samples were determined based on our
135 previous study²². The samples were dried in a conventional oven at 105 °C for 12 h, and the
136 moisture content (% wet basis) was calculated based on the weight loss observed after drying.

137 **2.4. Ash content**



138 The ash contents of aerogels were determined using the method followed by Liu ²³,
139 where the aerogel samples were heated in a muffle furnace (Barnstead Thermolyne 1400
140 Furnace, NY, USA) at 600 °C and left overnight. The ash contents of the samples were obtained
141 by calculating the total ash content as % sample mass (in dry basis).

142 **2.5. Density, porosity, and shrinkage**

143 The bulk density of the samples was measured using the weight-to-volume ratio by filling
144 a known weight of the sample into a measuring cylinder and recording its corresponding volume.
145 The true density was measured using a gas pycnometer (AccuPyc II 340, Micromeritics, GA,
146 USA) at room temperature (23 °C) in a 10 cm³ cell, with purge and cycle fill pressures
147 maintained at 19.5 psig. The porosity was calculated from bulk and true density using the
148 following Eq. 1:

$$149 \text{ Porosity (\%)} = \left(1 - \frac{\text{Bulk density}}{\text{True density}}\right) \times 100 \quad (1)$$

150 **2.6. Surface area, pore size, and pore volume**

151 The surface area, pore size, and volume of the aerogel were analyzed using a low-
152 temperature nitrogen adsorption–desorption (TriStar II Plus, Micromeritics Instrument
153 Corporation, GA, USA). Approximately 0.1–0.3 g of each aerogel sample was placed in the
154 sample tubes and degassed at 75 °C for 24 h ¹⁴. The nitrogen sorption measurements were
155 performed at –196 °C. The specific surface area was calculated using the multipoint Brunauer–
156 Emmett–Teller (BET) method within a relative pressure range (p/p_0) of 0.05–0.3, whereas the
157 Barrett–Joyner–Halenda (BJH) method was used to determine pore size and volume at relative
158 pressures above 0.35.

159 **2.7. Scanning electron microscopy**



160 The microstructural images of the aerogels were taken following the method outlined by
161 Sadaf, *et al.*²², using a FEI Nova Nanolab 200 Dual Beam system (FEI Company, OR, USA),
162 which is equipped with a 30 kV FIB column and 30 kV SEM FEG column. Prior to imaging, the
163 aerogel samples were coated in a gold layer at a deposition rate of 25 nm/min using an
164 EMITECH SC7620 Sputter Coater (MA, USA). The SEM analysis was performed at 15 kV and
165 15 mA in low-vacuum mode, with a working distance of 5 mm. The SEM images were captured
166 at magnifications of 500× and 5000×.

167 2.8. X-ray diffraction (XRD)

168 The XRD pattern of aerogels was analyzed using a high-resolution X-ray diffractometer
169 (Philips, Almelo, Netherlands), following the method of Sadaf, *et al.*²². The XRD
170 measurements were conducted at 45 kV and 40 mA, scanning over a 2θ range of 5° to 60° with a
171 step size of 0.02° and a scan speed of 0.0167 °/s.

172 2.9. Fourier Transform Infrared Spectroscopy

173 FTIR spectra of aerogel samples were recorded using a Shimadzu IRAffinity-1S
174 spectrometer equipped with a Quest ATR accessory. The spectral data were collected from 400
175 to 4000 cm⁻¹ with a resolution of 8 cm⁻¹ over 64 scans²⁴.

176 2.10. Water absorption

177 The water absorption capacity of aerogels was evaluated by following the method of
178 Silva, *et al.*²⁵. The samples were weighed before and after water immersion (1:50, w/v) for
179 about 24 h. The water absorption capacity was determined using Eq. 2:

$$180 \text{ Water absorption capacity (\%)} = \left(\frac{SW-DW}{DW} \right) \times 100$$

181 (2)

182 where SW and DW are the swollen and dry weight of the aerogel, respectively.



183 2.11 Methylene blue adsorption capacity

184 Methylene blue adsorption experiments were conducted based on the method followed by
 185 Nguyen, *et al.*²⁶ with minor modifications. Aerogel samples (0.05 g) were added to 50 mL
 186 methylene blue solution (15 mg/mL, pH 7) and maintained at 30 °C in a shaker bath operating at
 187 50 rpm. Aliquots of 2.5 mL were withdrawn at required time intervals (until equilibrium) and
 188 their absorbance measured at 665 nm using a spectrophotometer (Milton Roy Spectronic 1201
 189 spectrophotometer, PA, USA). The adsorption capacity at time (Q_t), the equilibrium adsorption
 190 capacity (Q_e), and methylene blue removal efficiency (R_e), were calculated using the following
 191 Eq. (3) and (4):

$$192 \quad Q_t(\text{mg/g}) = \frac{(C_0 - C_t) \times V}{m}$$

193 (3)

$$194 \quad Q_e(\text{mg/g}) = \frac{(C_0 - C_e) \times V}{m}$$

195 (4)

$$196 \quad R_e(\%) = \frac{(C_0 - C_e)}{C_0} \times 100$$

197 (5)

198 where C_0 , C_t , and C_e (mg/L) represent initial, time-dependent (min), and equilibrium
 199 concentration of methylene blue, respectively. V (L) is the volume of the methylene blue
 200 solution, and m (g) is the mass of the adsorbent.

201 2.12 Adsorption kinetics

202 To further understand the adsorption mechanism, the adsorption kinetics prediction of
 203 was evaluated using pseudo-first-order and second-order models expressed by Eq. (6) and (7)²⁷:

$$204 \quad \ln(q_e - q_t) = \ln q_e - k_1 \times t \quad (6)$$



$$\frac{t}{q_t} = \frac{1}{k_2 \times q_e^2} + \frac{1}{q_e} \times t \quad (7)$$

205 where q_e (mg/g) represents the amount of adsorbed methylene blue at equilibrium, q_t (mg/g)
 206 represents the amount of methylene blue adsorbed at time t , and k_1 (min^{-1}) and k_2 ($\text{g}/(\text{mg}\cdot\text{min})$)
 207 are the pseudo-first-order and second-order rate constants, respectively.

208 The initial adsorption rate v_0 ($\text{mg}/(\text{g}\cdot\text{min})$) at time 0 could be calculated by the following Eq. (8):

$$209 \quad v_0 = k_2 \times q_e^2 \quad (8)$$

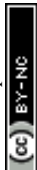
210 2.13. Statistical analysis

211 All measurements were taken in triplicate, and the results are presented as mean \pm
 212 standard deviation. Statistical analysis was performed using ANOVA in JMP Pro (Version
 213 17.0.0, SAS Institute, NC, USA), followed by Tukey's test with a significance of $p < 0.05$.

214 3. Results and discussion

215 3.1. Moisture content

216 The moisture content of the fresh samples was determined as $89.38 \pm 0.10\%$, $94.10 \pm$
 217 0.36% , $93.27 \pm 0.17\%$, $89.43 \pm 0.68\%$, and $74.73 \pm 0.04\%$ w.b for BPA, BSA, CLA, ICA, and
 218 OPA, respectively. The OPA had the lowest, and the BSA had the highest moisture content. The
 219 differences in moisture content among the fruit and vegetable waste samples can be attributed to
 220 their inherent tissue structure and composition²⁸. Moreover, the primary cell wall and middle
 221 lamella are most responsible for the texture and structure of fruits and vegetables²⁹. Most of the
 222 dry mass of the banana peel comes from its fiber content, made up of cellulose (7.6–9.6%),
 223 hemicellulose (10–21%), and lignin (6–12%)³⁰. In case of orange peels, the fibers include
 224 cellulose (22%), pectin (25%), and hemicellulose (11%) based on the percentage of whole peels
 225 ³¹⁻³³. The other fruit and vegetable waste, including carrots, cabbage leaves, and broccoli stems,
 226 had fiber content less than 3%³⁴. Within which the carrots had a water-insoluble polysaccharide



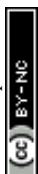
227 content including cellulose, hemicellulose, and lignin of 71.7%, 13.0%, and 15.2%, respectively
228 ³⁵. In broccoli stems, cellulose, hemicellulose, and pectin accounted for $18.5 \pm 2.1\%$, $24.1 \pm$
229 0.3% , and $57.8 \pm 2.8\%$, respectively ³⁶, whereas in cabbage leaves, cellulose, hemicellulose, and
230 lignin were the major components as $9.07 \pm 3.67\%$, $1.48 \pm 0.95\%$, and $9.82 \pm 3.56\%$,
231 respectively ³⁷. The composition of the fruits and waste vegetable samples largely influenced the
232 surface area of aerogels.

233 3.2. Ash content

234 The BPA ($8.16 \pm 0.45\%$) had the highest ash content, while the OPA ($3.08 \pm 0.70\%$) had
235 the lowest (Table 1). The variation in ash content represents the difference in mineral content in
236 the fruit and vegetable waste samples. Similar results were reported by Zhang, *et al.* ³⁸, where
237 the banana peels had the highest ash content, while the orange peels had the lowest. The presence
238 of ash content can be correlated to the thermal resistance of aerogels. For example, in a study by
239 Khodavandegar, *et al.* ³⁹ investigating chitosan-lignin aerogels, the authors reported that the
240 composite with higher ash content (reflecting more inorganic or char-forming content) produced
241 higher char yield and better thermal resistance during decomposition.

242 3.3. Density and porosity

243 The SC-CO₂-dried aerogels from different fruit and vegetable waste sources are
244 presented in Fig. 1. The true density almost remained the same ($\sim 1.45 \pm 0.01 \text{ g/cm}^3$) across all
245 samples except for cabbage and carrot, which had slightly higher density values ($\sim 1.49 \text{ g/cm}^3$).
246 The variation in true density may result from changes in molecular or structural arrangements,
247 which may occur during a second-order phase transition influenced by its thermal history ⁴⁰. The
248 bulk density of the aerogels ($\sim 0.1 \text{ g/cm}^3$) showed minimal variation across samples. In contrast,
249 porosity values varied significantly ($p < 0.05$). The porosity as high as above 90% is a



250 characteristic of aerogels for its utilization in food applications, including thermal insulations in
251 packaging, carriers for flavors, nutrients, fat and sugar replacers, and texture enhancers. Their
252 high porosity, low density, and varied surface properties make them ideal for encapsulation and
253 controlled release of bioactive compounds ⁴¹. Similar to these results, Gibowsky, *et al.* ²,
254 reported high-porosity values above 97% for food-waste aerogels derived from natural fruit and
255 vegetable tissues, demonstrating their strong potential for application in oleogelation. The study
256 assessed 20 different tissues, including apple, pear, plum, banana peel, orange peel, orange pulp,
257 kiwi, radish, carrot, bell pepper, cucumber, tomato, onion, nectarine, strawberry, mushroom, and
258 others. The study utilized fresh tissues that were washed, shredded, or pulp removed, solvent-
259 exchanged using ethanol, and then dried using SC-CO₂, converting the native cellular
260 architecture to porous aerogels. The resulting aerogels were then categorized into three structural
261 groups based on their pore-size distributions including category 1 with primarily small
262 mesopores (pore diameter ≤ 6.5 nm), category 2 with mixed mesopore populations (with pore
263 diameters small (≤ 6.5 nm), mid (≈ 6.5 – 10 nm), and larger mesopores (≈ 10 – 50 nm)), and
264 category 3 dominated by larger mesopores (pore diameter 10–50 nm). Irrespective of the
265 category, all samples had a high porosity above 97%.

266 3.4. Surface area, pore size, and pore volume

267 The OPA samples had the highest surface area (171.78 ± 6.67 m²/g), followed by BPA
268 (57.37 ± 4.64 m²/g), ICA (55.35 ± 12.24 m²/g), BSA (23.50 ± 3.26 m²/g), and CLA ($12.21 \pm$
269 3.27 m²/g) (Table 1). The pore size volume was also high in the case of OPA (0.45 ± 0.01
270 cm³/g). The higher pore size and surface area of the OPA can be attributed to the presence of
271 fibrils within the microstructure of OPA samples. Moreover, the high surface area of OPA can
272 also be attributed to its composition, which contains a high amount of pectin and cellulose ¹⁵.



273 The presence of cellulose with insoluble fibers contributes to the development of a large surface
274 area⁴². Following OPA, the BPA samples had a high surface area, likely due to the presence of
275 similar constituents such as cellulose and pectin that contribute to pore formation and fibrous
276 network; however, the surface area of BPA was lower than that of the OPA, attributing to varied
277 cellulose content^{43, 44}.

278 Next to BPA ($57.37 \pm 4.64 \text{ m}^2/\text{g}$), ICA ($55.35 \pm 12.24 \text{ m}^2/\text{g}$) had a higher surface area,
279 which can be attributed to the presence of higher cellulose content in carrots. Shih, *et al.*⁴⁵
280 produced bio-aerogels from cellulose nanofibers extracted from carrot pulp and reported a
281 porous structure with a large surface area, demonstrating excellent swelling capacity. The high
282 surface area of ICA can also be attributed to the presence of soluble and insoluble fibers present
283 in carrot samples⁴⁶. The presence of soluble fibers can enhance the porosity as it attracts water
284 to form a gel matrix, while the insoluble fibers also form a matrix; however, it does not expand
285 in water⁴⁷. The BSA and CLA samples had the lowest surface area of $23.50 \pm 3.26 \text{ m}^2/\text{g}$ and
286 $12.21 \pm 3.27 \text{ m}^2/\text{g}$, respectively. It can be due to the significantly higher water content present in
287 these samples when compared to other fruit and vegetable waste samples. Dourbash, *et al.*⁴⁸
288 concluded that higher initial water content decreased the surface area and porosity of silica
289 aerogel samples. When the water content is lower, the surface is more likely to undergo complete
290 chemical modification, leading to the “spring-back effect,” which consequently reduces the
291 volume shrinkage^{49, 50}. Moreover, the pore size of the BSA and CLA was also large,
292 demonstrating the lower surface area. This is because a material with larger pores will have
293 fewer pores in a given volume compared to a material with smaller pores, and the total surface
294 area is the sum of the area of all the pores. A material with many smaller pores will have a higher
295 total internal surface area⁵¹.



296

297 **Table 1.** Ash content, density, porosity, surface area, pore volume, pore size, and water

298 absorption capacity of fruit and vegetable waste aerogels.

Aerogel Sample	BPA	BSA	CLA	ICA	OPA
Ash content (%)	8.16 ± 0.45 ^a	7.26 ± 0.41 ^{ab}	5.25 ± 1.28 ^{bc}	6.36 ± 0.03 ^{ab}	3.08 ± 0.70 ^c
True density (g/cm ³)	1.46 ± 0.01 ^b	1.46 ± 0.01 ^b	1.50 ± 0.004 ^a	1.49 ± 0.01 ^a	1.44 ± 0.01 ^b
Bulk density (g/cm ³)	0.08 ± 0.01 ^a	0.08 ± 0.02 ^a	0.11 ± 0.06 ^a	0.10 ± 0.01 ^a	0.10 ± 0.0001 ^a
Porosity (%)	94.69 ± 0.02 ^a	94.57 ± 0.02 ^b	92.53 ± 0.02 ^c	93.22 ± 0.03 ^d	93.41 ± 0.03 ^c
BET surface area (m ² /g)	57.37 ± 4.64 ^b	23.50 ± 3.26 ^c	12.21 ± 3.27 ^c	55.35 ± 12.24 ^b	171.78 ± 6.67 ^a
Pore volume (cm ³ /g)	0.21 ± 0.002 ^b	0.11 ± 0.01 ^{cd}	0.08 ± 0.01 ^d	0.15 ± 0.03 ^c	0.45 ± 0.01 ^a
Pore size (nm)	14.35 ± 1.52 ^b	19.19 ± 0.60 ^{ab}	28.79 ± 6.78 ^a	9.83 ± 0.46 ^b	9.17 ± 0.23 ^b
Water absorption capacity (%)	1127.7 ± 17.39 ^c	2006.8 ± 3.68 ^a	2038.1 ± 0.42 ^a	1600 ± 118.79 ^b	674.2 ± 50.91 ^d

299 †Means ± standard deviation bars that do not share a common letter within each property (row)

300 are significantly different ($p < 0.05$). BPA: Banana peel aerogel; BSA: Broccoli stem aerogel;

301 CLA: Cabbage leaf aerogel; ICA: Imperfect carrot aerogel, and OPA: Orange peel aerogel.

302

303 **3.5. Morphology**

304 The SEM images of the aerogels (Fig. 2) revealed a well-defined porous structure with
305 intact hexagonal cell arrangements, confirming that SC-CO₂ drying effectively preserved the
306 microstructure of all the samples. Among the samples, CLA samples had noticeably larger pores,
307 whereas OPA, BPA, and ICA depicted smaller macropores. The larger pore size observed in
308 CLA can be useful for adsorption, especially in biomedical applications¹⁶, further supported by
309 the relatively high surface area of these samples. At higher magnification, OPA and BPA
310 samples revealed fine fibrillar networks, with OPA showing more extensive fibrillation, which
311 contributes to the higher surface area of these samples. The high surface area of aerogels enables
312 a wide range of applications, including adsorption and filtration, drug delivery, and other
313 biomedical applications, as well as thermal insulation⁵².

314 3.6. Crystallinity

315 The aerogel samples exhibited an amorphous nature in general, with varied crystallinity
316 among different aerogel samples (Fig. 3a). The OPA and BPA samples exhibited sharp
317 diffraction peaks around 15°, 17°, 22°, and 35° 2θ angle, indicating the presence of crystalline
318 cellulose components⁵³. The observed crystallinity can be attributed to the hydrogen bonding
319 interactions and van der Waals forces between adjacent molecules, whereas the remaining lignin
320 and cellulose components exhibited a more amorphous nature⁵⁴. The ICA and BSA had sharp
321 peaks near 21.5° 2θ angle, indicating the presence of pectin^{55,56}. The pectin typically exists in
322 an amorphous or semi-crystalline state, due to hydrogen bonding among hydroxyl groups within
323 the polysaccharide chain⁵⁷. Even though the BSA and ICA samples displayed the presence of
324 ordered structure, it was less pronounced compared to the peel samples, OPA and BPA. In
325 contrast, the CLA samples did not display a distinct, sharp peak but rather a broader peak near



326 21.5°, which could represent lignin present in the samples, which also presented a broad
327 amorphous peak centered around 21.5°⁵⁸.

328 3.7. Chemical interaction

329 The FTIR spectra provided information on the functional groups present in the aerogels
330 (Fig. 3b), where typical lignocellulosic material characteristics were observed. All the samples
331 had a broad peak near 3100-3600 cm⁻¹, representing the –OH stretching vibration. Among all the
332 samples, CLA had a broader peak, representing a strong hydrogen bonding interaction. In
333 addition, the aerogels exhibited peaks near 2920 and 2850 cm⁻¹, corresponding to the asymmetric
334 and symmetric stretching vibrations of C–H bonds⁵⁹. The peaks at 2850 cm⁻¹ were more visible
335 in the CLA, possibly due to a higher content of aliphatic C–H groups derived from lipids or
336 cuticular wax components present in cabbage leaves, which remained during aerogel formation
337⁶⁰. Further, the peak around 1735 cm⁻¹ corresponded to the stretching vibration of the carboxyl
338 functional group C=O ester bond. In plant cells, this absorption is mainly attributed to the
339 esterified carboxyl groups in pectin (methyl esters of galacturonic acid) or other ester-containing
340 components. The FTIR spectra showed that the OPA and CLA samples exhibited stronger peaks
341 near 1735 cm⁻¹, suggesting a higher content of esterified compounds, whereas the BSA, ICA, and
342 BPA samples displayed much weaker peaks, indicating a lower degree or possible absence of
343 these ester groups^{58, 61}.

344 The region from 1600 to 1321 cm⁻¹ is dominated by carboxylate (–COO⁻) vibrations. The
345 band near 1600–1585 cm⁻¹ corresponded to the aromatic rings of C=C stretching, while the peaks
346 at 1415 and 1315 cm⁻¹ were due to symmetric –COO⁻ stretching and C–O (~1050 cm⁻¹)
347 deformation vibrations⁵³. These features indicate the presence of carboxylate-containing
348 polysaccharides, such as pectin and hemicellulose, which were more prominent in CLA, BSA,



349 and ICA, reflecting their amorphous nature. In contrast, BPA and OPA, which contained higher
350 cellulose content, exhibited slightly weaker and narrower peaks, consistent with increased
351 structural ordering ⁶².

352 3.8. Water absorption capacity

353 All the aerogel samples had a high-water absorption capacity, exceeding 670% (Table 1).
354 Among them, CLA and BSA showed the highest absorption (~2000%), which can be attributed
355 to their larger pore sizes facilitating greater water absorption. Yin, *et al.* ⁶³ reported similar
356 trends in Balsa wood aerogels, where larger pore sizes enabled faster absorption rate and greater
357 absorption capacity. The ICA samples also demonstrated high water absorption (1600%), likely
358 due to their porosity and their high ratio of soluble fibers, which enhance water retention by
359 forming a gel network. This is consistent with the findings of Shih, *et al.* ⁴⁵, who reported high
360 water absorption up to 1100% in carrot pulp aerogels. In contrast, the peel samples, BPA, and
361 OPA had slightly lower water absorption capacity of $1127.7 \pm 17.39\%$ and $674.2 \pm 50.91\%$ than
362 non-peel samples, including BSA ($2006.8 \pm 3.68\%$), CLA ($2038.1 \pm 0.42\%$), and ICA ($1600 \pm$
363 118.79%), respectively. This can be attributed to their higher content of insoluble fibers, which
364 limit water uptake ⁶⁴. These results are in agreement with earlier studies as reported by
365 Wanlapa, *et al.* ⁶⁵. Water absorption capacity can play important roles in food applications like
366 active and intelligent food packaging, moisture control to extend shelf life, and absorbent pads
367 for exudate management in fresh products. It can also be valuable in other applications, including
368 atmospheric water harvesting and environmental cleanup, like water purification and separation
369 for their high porosity, large surface area, and tunable hydrophilicity ^{66, 67}.

370 3.9 Methylene blue adsorption capacity



371 The methylene blue adsorption capacity of aerogel samples is represented in Fig. 4. The
372 methylene blue removal efficiency of BPA, BSA, CLA, ICA, and OPA was $87.99 \pm 0.10\%$,
373 $80.77 \pm 0.16\%$, $78.59 \pm 0.10\%$, $87.99 \pm 0.38\%$, and $53.49 \pm 0.32\%$, respectively. The removal
374 efficiency of the OPA was the lowest when compared to other samples, which can be directly
375 correlated to the microstructure of OPA, providing lower water and dye adsorption capacity.
376 Despite the highest BET specific surface area of OPA, it showed lower methylene blue
377 adsorption capacity compared to all samples. The adsorption performance is strongly influenced
378 by pore size distribution and surface chemistry. In the OPA, a significant fraction of the surface
379 area is likely associated with micropores (as indicated in SEM) that are not accessible to the
380 relatively large methylene blue molecules, thereby limiting effective adsorption. Michael
381 Igolima, *et al.*⁶⁸ also reported lower adsorption capacity of raw orange peels when compared to
382 physically modified orange peels, which have increased the porous structure for the adsorption of
383 contaminants. In accordance with this, the BPA and ICA, having moderate surface area with
384 mesopores, had the highest methylene blue adsorption. Similar observations were concluded by
385 Zhou, *et al.*⁶⁹, where ultra-high surface area mesoporous carbon facilitated faster and more
386 effective adsorption for bulk molecules like methyl blue compared to larger mesopores and
387 microporous materials. In the case of BSA and CLA, the SEM morphology shows a large pore
388 size, resulting in reduced methylene blue adsorption than ICA and BPA.

389 3.10 Adsorption kinetics

390 The value of adsorption kinetic parameters was assessed from the plots of pseudo-first
391 order, and pseudo-second order linear plots (Fig. 5). These models help in predicting the
392 equilibrium adsorption kinetics and identify the surface adsorption mechanism of methylene blue
393 on aerogels⁷⁰. In the initial stages of adsorption, till 120 min, there was an increase in adsorption



394 capacity, which is 80% of the adsorption capacity, and later became constant. Methyl blue, being
395 a cationic dye in aqueous solution, interacts electrostatically with adsorption sites such as –OH
396 and –COOH functional groups present on the surfaces of aerogels in the adsorbent. Due to the
397 availability of more active sites for methylene blue adsorption, the initial adsorption rate is
398 higher; however, as time progresses, these free active sites diminish, resulting in a decreased
399 adsorption rate ⁷¹. The adsorption of methylene blue is governed by multiple interaction
400 mechanisms, including π – π interactions, hydrogen bonding, surface complexation, electrostatic
401 interactions, ion exchange processes, and van der Waals forces ⁷². While electrostatic attraction
402 between the cationic dye and negatively charged surface groups is a probable pathway for fruits
403 and vegetable waste, other interactions also play significant roles ⁷³. The presence of hydroxyl,
404 and carboxyl groups (as evidenced by FTIR analysis) facilitates adsorption through hydrogen
405 bonding and surface interactions. In addition, π – π interactions between the aromatic structure of
406 methylene blue and lignin-derived components of the fruits and vegetable waste may also
407 contribute to adsorption ⁷⁴. Moreover, the highly porous structure of the aerogels further
408 facilitates pore-filling and physical adsorption. Table 2 presents the kinetic model parameters
409 calculated from the pseudo-first-order and second-order models (Fig. 5). From Table 2, it can be
410 observed that the correlation coefficients (R^2) for all the aerogels were higher for the pseudo-
411 first-order than the second-order kinetic curve, except for OPA, indicating that the adsorption
412 involved chemical reactions (or chemisorption) in addition to physisorption ⁷⁵. The pseudo-
413 second-order kinetic behavior suggests that the adsorption process is governed by interactions
414 between the adsorbate and available active sites on the adsorbent surface. In OPA, this behavior
415 can arise from the presence of abundant functional groups (e.g., hydroxyl and carboxyl groups),
416 which facilitate multiple interaction mechanisms including hydrogen bonding, electrostatic



417 attraction, and surface complexation. However, it is important to note that pseudo-second-order
418 kinetics does not exclusively confirm chemisorption but rather indicates that the adsorption rate
419 is controlled by the availability and reactivity of surface sites ⁷⁶. Despite exhibiting the highest
420 BET surface area, the adsorption rate was low, due to enhanced interaction of the abundant
421 functional group with the cationic methylene blue dye, leading to surface-controlled adsorption
422 consistent with pseudo-second-order kinetics ⁷⁷. Furthermore, the porous structure may introduce
423 diffusion limitations, particularly within smaller pores, which further reduces the overall
424 adsorption rate. Khumalo, *et al.* ⁷⁶ explained that adsorption performance is governed more by
425 functional group availability and pore accessibility than by surface area alone, with the
426 carboxymethyl cellulose-based silica aerogel providing more accessible binding sites and better
427 diffusion pathways for methylene blue despite its lower BET surface area. For other food waste
428 aerogels, the results identified that the pseudo-first-order kinetic model was more appropriate for
429 describing the adsorption kinetics, favoring the surface area results. These results are consistent
430 with previous studies, which reported that the methylene blue adsorption behavior of chitosan
431 aerogels was better described by the pseudo-first-order model than by the pseudo-second-order
432 model ⁷⁸. Moreover, the predicted q_e and v_0 were almost equivalent to the experimental results,
433 confirming the suitability of the proposed model for describing methylene blue adsorption of
434 food waste aerogels.

435

436 **Table 2.** Kinetic parameters of pseudo-first-order kinetics and pseudo-second-order kinetics of
437 methylene blue adsorption of aerogels

Pseudo first-order kinetics



Kinetic Parameters	BPA	BSA	CLA	ICA	OPA
q_e (mg/g)	8.34	8.68	8.05	8.24	7.42
k_1 (min ⁻¹)	0.0168	0.0176	0.0136	0.02	0.0292
R^2	0.9797	0.9768	0.9646	0.9982	0.8619

Pseudo-second order kinetics					
Kinetic Parameters	BPA	BSA	CLA	ICA	OPA
q_e (mg/g)	8.95	9.50	9.29	9.12	5.84
k_2 (g/(mg·min))	0.0027	0.0014	0.0012	0.0029	0.0035
R^2	0.9611	0.87	0.828	0.9693	0.9423
v_0 (mg/(g·min))	0.22	0.12	0.10	0.24	0.12

438

439 **4. Conclusions**

440 Nearly one-third of the world's food is lost, with fruits and vegetables being the most
 441 wasted despite their nutritional value. Producing aerogels from fruit and vegetable waste
 442 provides an effective upcycling route to convert this biomass into high-value materials. In this
 443 study, aerogels were prepared from BPA, BSA, CLA, ICA, and OPA. All aerogels exhibited
 444 highly porous structures, with densities below 0.1 g/cm³, porosities above 93%, and high surface
 445 areas (12 m²/g -172 m²/g). The peel samples showed the highest BET surface areas, reaching
 446 ~172 m²/g for OPA and ~57 m²/g for BPA. The pore size results revealed that CLA samples
 447 exhibited the largest pores, with an average BJH pore size of ~29 nm, which contributed to their
 448 highest water absorption capacity of 2000%. Crystallinity analysis indicated that the aerogels



449 were predominantly amorphous, although OPA and BPA displayed relatively higher crystalline
450 features, likely due to the presence of a cellulosic structure. FTIR spectra confirmed the presence
451 of pectin, cellulose, and hemicellulose in all samples, with variations among the different fruit
452 and vegetable sources. The methylene blue adsorption capacity was largely driven by
453 electrostatic interaction, with an average adsorption capacity of ~84% except for OPA (53%).
454 The pseudo-first order kinetics model better predicted the methylene blue adsorption kinetics
455 compared to the pseudo-second order model, with $R^2 > 0.98$. Overall, this study demonstrates
456 that fruit and vegetable waste can be effectively used as whole materials for aerogel production.
457 This work minimizes the pretreatments needed to create biopolymer-based aerogels.

458 **CRedit authorship contribution statement**

459 Niveditha Asaithambi: Methodology, Validation, Formal Analysis, Writing –
460 Original Draft, Visualization. Ali Ubeyitogullari: Conceptualization, Methodology, Supervision,
461 Validation, Writing – Review & Editing, Project Administration, Funding Acquisition,
462 Resources.

463 **Declaration of competing interest**

464 There are no conflicts of interest to declare.

465 **Data availability statement**

466 The data supporting this article have been included as part of the current article.

467 **Acknowledgements**

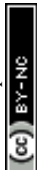
468 This project was supported, at least in part, by the USDA National Institute of Food and
469 Agriculture, Multistate Project NC1023, Accession number 1025907, AFRI award no: 2023-
470 67022-40164, and EGP 2024-70410-43765.

471 **References**

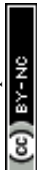
472



- 473 1. FAO, Food Wastage Footprint Full-cost Accounting, Final Report, 9251085129, Food &
474 Agriculture Organization of the UN (FAO), Rome, Italy, 2014.
- 475 2. L. Gibowsky, L. De Berardinis, S. Plazzotta, E. Manke, I. Jung, D. A. Méndez, F.
476 Heidorn, G. Liese, J. Husung, A. Liese, P. Gurikov, I. Smirnova, L. Manzocco and B.
477 Schroeter, *Green Chemistry*, 2025, 27, 4713-4731, DOI: 10.1039/d4gc05703a.
- 478 3. L. Cassani and A. Gomez-Zavaglia, *Frontiers in Nutrition*, 2022, 9, DOI:
479 10.3389/fnut.2022.829061.
- 480 4. A. Niveditha, D. V. Chidanand and C. K. Sunil, *Measurement: Food*, 2023, 12, DOI:
481 10.1016/j.meaf00.2023.100114.
- 482 5. R. Karmakar, S. Aggarwal, D. Kathuria, N. Singh, V. Tripathi, P. K. Sharma, D. Mitra, S.
483 Kumar and S. Bhattacharya, *Food Bioscience*, 2025, 69, DOI:
484 10.1016/j.fbio.2025.106833.
- 485 6. A. A. Zaky, D. Witrowa-Rajchert and M. Nowacka, *Food Safety and Health*, 2025, 3,
486 315-333, DOI: 10.1002/fsh3.70012.
- 487 7. W. A. El-Fattah, A. Guesmi, N. Ben Hamadi, M. G. El-Desouky and A. Shahat, *Colloids
488 and Surfaces A: Physicochemical and Engineering Aspects*, 2024, 681, DOI:
489 10.1016/j.colsurfa.2023.132729.
- 490 8. N. Saad, M. Al-Mawla, E. Moubarak, M. Al-Ghoul and H. El-Rassy, *RSC Advances*,
491 2015, 5, 6111-6122, DOI: 10.1039/c4ra15504a.
- 492 9. M. G. El-Desouky, M. A. G. Khalil, M. A. M. El-Afify, A. A. El-Bindary and M. A. El-
493 Bindary, *Desalination and Water Treatment*, 2022, 280, 89-127, DOI:
494 10.5004/dwt.2022.29029.
- 495 10. A. Ubeyitogullari, S. Ahmadzadeh, G. Kandhola and J. W. Kim, *Comprehensive
496 Reviews in Food Science and Food Safety*, 2022, 21, 4610-4639, DOI: 10.1111/1541-
497 4337.13049.
- 498 11. L. Manzocco, K. S. Mikkonen and C. A. García-González, *Food Structure*, 2021, 28,
499 DOI: 10.1016/j.foostr.2021.100188.
- 500 12. H. P. S. Abdul Khalil, E. Bashir Yahya, F. Jummaat, A. S. Adnan, N. G. Olaiya, S. Rizal,
501 C. K. Abdullah, D. Pasquini and S. Thomas, *Progress in Materials Science*, 2023, 131,
502 DOI: 10.1016/j.pmatsci.2022.101014.
- 503 13. S. Kaur, J. Chen and A. Ubeyitogullari, *Sustainable Food Proteins*, 2025, 3, DOI:
504 10.1002/sfp2.70011.
- 505 14. S. Ahmadzadeh and A. Ubeyitogullari, *Carbohydrate Polymers*, 2023, 301, DOI:
506 10.1016/j.carbpol.2022.120296.
- 507 15. L. T. Possari, P. F. Ávila, M. Brienzo, C. G. Otoni, T. Budtova and S. H. P. Bettini, *ACS
508 Sustainable Resource Management*, 2025, 2, 944-952, DOI:
509 10.1021/acssusresmg.4c00511.
- 510 16. S. Karamikamkar, E. P. Yalcintas, R. Haghniaz, N. R. de Barros, M. Mecwan, R. Nasiri,
511 E. Davoodi, F. Nasrollahi, A. Erdem, H. Kang, J. Lee, Y. Zhu, S. Ahadian, V. Jucaud, H.
512 Maleki, M. R. Dokmeci, H. J. Kim and A. Khademhosseini, *Advanced Science*, 2023, 10,
513 DOI: 10.1002/advs.202204681.
- 514 17. J. Yan, S. Jiang, C. Lin, W. Wang, L. Liu, H. Tang and R. Guo, *International Journal of
515 Biological Macromolecules*, 2025, 322, DOI: 10.1016/j.ijbiomac.2025.146476.
- 516 18. M. Kloster, M. A. Mosiewicki and N. E. Marcovich, *International Journal of Biological
517 Macromolecules*, 2025, 329, DOI: 10.1016/j.ijbiomac.2025.147764.



- 518 19. M. He, Y. Huang, Z. Cui, Z. Cheng, W. Cao, G. Wang, W. Yao and M. Feng, *Gels*, 2026,
519 12, DOI: 10.3390/gels12010076.
- 520 20. M. Jentzsch, V. Albiez, T. C. Kardamakis and T. Speck, *Soft Matter*, 2024, 20, 2804-
521 2811, DOI: 10.1039/d3sm01511d.
- 522 21. H. Kumar, K. Bhardwaj, R. Sharma, E. Nepovimova, K. Kuča, D. S. Dhanjal, R. Verma,
523 P. Bhardwaj, S. Sharma and D. Kumar, *Molecules*, 2020, 25, DOI:
524 10.3390/molecules25122812.
- 525 22. N. Sadaf, A. Tuhanioglu, N. Hettiarachchy and A. Ubeyitogullari, *RSC Advances*, 2024,
526 14, 5851-5862, DOI: 10.1039/d3ra07426a.
- 527 23. K. Liu, *Algal Research*, 2019, 40, DOI: 10.1016/j.algal.2019.101486.
- 528 24. M. D. R. Lenie, S. Ahmadzadeh, F. Van Bockstaele and A. Ubeyitogullari, *Food*
529 *Hydrocolloids*, 2024, 153, DOI: 10.1016/j.foodhyd.2024.109989.
- 530 25. F. T. Silva, L. M. Fonseca, G. P. Bruni, R. L. Crizel, E. G. Oliveira, E. d. R. Zavareze
531 and A. R. G. Dias, *International Journal of Biological Macromolecules*, 2023, 249, DOI:
532 10.1016/j.ijbiomac.2023.126108.
- 533 26. V. T. Nguyen, L. Q. Ha, T. D. L. Nguyen, P. H. Ly, D. M. Nguyen and D. Hoang, *ACS*
534 *Omega*, 2021, 7, 1003-1013, DOI: 10.1021/acsomega.1c05586.
- 535 27. Z. Yu, C. Hu, A. B. Dichiaro, W. Jiang and J. Gu, *Nanomaterials*, 2020, 10, DOI:
536 10.3390/nano10010169.
- 537 28. Y. Li, H. Zhao, K. Xiang, D. Li, C. Liu, H. Wang, W. Pang, L. Niu, R. Yu and X. Sun,
538 *Journal of Food Engineering*, 2024, 365, DOI: 10.1016/j.jfoodeng.2023.111828.
- 539 29. D. Heaney and O. I. Padilla-Zakour, *Foods*, 2025, 14, DOI: 10.3390/foods14183267.
- 540 30. S. Mishra, B. Prabhakar, P. S. Kharkar and A. M. Pethe, *ACS Omega*, 2022, 8, 1140-
541 1145, DOI: 10.1021/acsomega.2c06571.
- 542 31. S. Gaiind, *Waste and Biomass Valorization*, 2016, 8, 1351-1360, DOI: 10.1007/s12649-
543 016-9682-2.
- 544 32. J. A. Dávila, M. Rosenberg and C. A. Cardona, *Waste and Biomass Valorization*, 2015,
545 6, 253-261, DOI: 10.1007/s12649-014-9339-y.
- 546 33. J. Ángel Siles López, Q. Li and I. P. Thompson, *Critical Reviews in Biotechnology*,
547 2010, 30, 63-69, DOI: 10.3109/07388550903425201.
- 548 34. B. Enkhmaa, P. Surampudi, E. Anuurad and L. Berglund, in *Endotext*, eds. K. R.
549 Feingold, S. F. Ahmed, B. Anawalt, M. R. Blackman, A. Boyce, G. Chrousos, E. Corpas,
550 W. W. de Herder, K. Dhatariya, K. Dungan, J. Hofland, S. Kalra, G. Kaltsas, N. Kapoor,
551 C. Koch, P. Kopp, M. Korbonits, C. S. Kovacs, W. Kuohung, B. Laferrère, M. Levy, E.
552 A. McGee, R. McLachlan, R. Muzumdar, J. Purnell, R. Rey, R. Sahay, A. S. Shah, F.
553 Singer, M. A. Sperling, C. A. Stratakis, D. L. Trence and D. P. Wilson, MDText.com,
554 Inc. Copyright © 2000-2025, MDText.com, Inc., South Dartmouth (MA), 2000.
- 555 35. K. D. Sharma, S. Karki, N. S. Thakur and S. Attri, *Journal of Food Science and*
556 *Technology*, 2011, 49, 22-32, DOI: 10.1007/s13197-011-0310-7.
- 557 36. V. Núñez-Gómez, R. González-Barrío, N. Baenas, D. A. Moreno and M. J. Periago,
558 *International Journal of Molecular Sciences*, 2022, 23, DOI: 10.3390/ijms232113309.
- 559 37. K. Rodkantuk, N. Chiewchan and S. Devahastin, *International Journal of Food Science &*
560 *Technology*, 2021, 56, 4316-4327, DOI: 10.1111/ijfs.15234.
- 561 38. J. Zhang, S. Hu, Y. Ding, R. Huang, Q. Ren, S. Su, Y. Wang, L. Jiang, J. Xu and J.
562 Xiang, *Processes*, 2023, 11, DOI: 10.3390/pr11030892.



- 563 39. S. Khodavandegar, R. Zare and P. Fatehi, *Industrial Crops and Products*, 2025, 234, DOI:
564 10.1016/j.indcrop.2025.121540.
- 565 40. A. López Ortiz, J. Rodríguez Ramírez and L. L. Méndez Lagunas, *International Journal*
566 *of Food Properties*, 2013, 16, 1516-1529, DOI: 10.1080/10942912.2011.599090.
- 567 41. A. Asqardokht-Aliabadi, J. Mohammadzadeh Milani and A. Dufresne, *Journal of*
568 *Agriculture and Food Research*, 2025, 24, DOI: 10.1016/j.jafr.2025.102331.
- 569 42. O. Korhonen and T. Budtova, *Composites Part A: Applied Science and Manufacturing*,
570 2020, 137, DOI: 10.1016/j.compositesa.2020.106027.
- 571 43. X. Yue, T. Zhang, D. Yang, F. Qiu and Z. Li, *Journal of Cleaner Production*, 2018, 199,
572 411-419, DOI: 10.1016/j.jclepro.2018.07.181.
- 573 44. F. Bigi, E. Maurizzi, H. Haghghi, H. Siesler, F. Licciardello and A. Pulvirenti, *Foods*,
574 2023, 12, DOI: 10.3390/foods12050960.
- 575 45. Y. F. Shih, T. Y. Pan, T. Y. Lu, T. H. Huang and C. W. Chang, *Waste Management*
576 *Bulletin*, 2025, 3, DOI: 10.1016/j.wmb.2025.100258.
- 577 46. X. Li, L. Wang, P. Jiang, Y. Zhu, W. Zhang, R. Li and B. Tan, *Lwt*, 2023, 173, DOI:
578 10.1016/j.lwt.2022.114304.
- 579 47. Z. Wang, H. Huang, Y. Wang, M. Zhou and W. Zhai, *Materials*, 2023, 17, DOI:
580 10.3390/ma17010172.
- 581 48. A. Dourbash, S. Motahari and H. Omranpour, *Journal of Non-Crystalline Solids*, 2014,
582 405, 135-140, DOI: 10.1016/j.jnoncrysol.2014.09.013.
- 583 49. H. Omranpour and S. Motahari, *Journal of Non-Crystalline Solids*, 2013, 379, 7-11, DOI:
584 10.1016/j.jnoncrysol.2013.07.025.
- 585 50. S. D. Bhagat, C.-S. Oh, Y.-H. Kim, Y.-S. Ahn and J.-G. Yeo, *Microporous and*
586 *Mesoporous Materials*, 2007, 100, 350-355, DOI: 10.1016/j.micromeso.2006.10.026.
- 587 51. S. J. Eichhorn and W. W. Sampson, *Journal of The Royal Society Interface*, 2009, 7, 641-
588 649, DOI: 10.1098/rsif.2009.0374.
- 589 52. H. Fan, B. Xue, J. Lu, T. Sun, Q. Zhao, Y. Liu, M. Niu, S. Yu, Y. Yang and L. Zhang,
590 *International Journal of Biological Macromolecules*, 2025, 291, DOI:
591 10.1016/j.ijbiomac.2024.139144.
- 592 53. F. Tomul, Y. Arslan, F. T. Başoğlu, Y. Babuçcuoğlu and H. N. Tran, *Journal of*
593 *Environmental Management*, 2019, 238, 296-306, DOI: 10.1016/j.jenvman.2019.02.088.
- 594 54. N. Johar, I. Ahmad and A. Dufresne, *Industrial Crops and Products*, 2012, 37, 93-99,
595 DOI: 10.1016/j.indcrop.2011.12.016.
- 596 55. K. Gao, B. Liu, B. Wu, Y. Guo, C. Song, S. Nan, J. Dai, Y. Shen and H. Ma, *Agriculture*,
597 2024, 14, DOI: 10.3390/agriculture14060803.
- 598 56. S. Ma, Z. Yang, H. Sun, T. Wu, S. Pan and X. Xu, *International Journal of Biological*
599 *Macromolecules*, 2025, 330, DOI: 10.1016/j.ijbiomac.2025.148164.
- 600 57. W. L. Liang, J. S. Liao, J. R. Qi, W. X. Jiang and X. Q. Yang, *Food Chemistry*, 2022,
601 375, 131806, DOI: 10.1016/j.foodchem.2021.131806
- 602 58. Ş. O. Dima, D. Constantinescu Aruxandei, N. Tritean, M. Ghiurea, L. Capră, C. A.
603 Nicolae, V. Faraon, C. Neamtu and F. Oancea, *Plants*, 2023, 12, DOI:
604 10.3390/plants12163016.
- 605 59. L. Chen, H. Zhang and X. Sui, *International Journal of Biological Macromolecules*, 2025,
606 327, DOI: 10.1016/j.ijbiomac.2025.147551.



- 607 60. W. Luo, E. Gonzalez, A. Zarei, S. Calleja, B. Rozzi, J. Demieville, H. Li, M.-J. Truco, D.
608 Lavelle, R. Michelmore, J. M. Dyer, M. A. Jenks and D. Pauli, *Heliyon*, 2024, 10, DOI:
609 10.1016/j.heliyon.2024.e27226.
- 610 61. J. López Mercado, A. Nambo, M. E. Toribio Nava, O. Melgoza Sevilla, L. Cázarez
611 Barragán, L. Cajero Zul, L. G. Guerrero Ramírez, B. E. Handy and M. G. Cardenas
612 Galindo, *Clean Technologies and Environmental Policy*, 2018, 20, 1413-1422, DOI:
613 10.1007/s10098-018-1570-y.
- 614 62. J. Müller-Maatsch, M. Bencivenni, A. Caligiani, T. Tedeschi, G. Bruggeman, M. Bosch,
615 J. Petrusan, B. Van Droogenbroeck, K. Elst and S. Sforza, *Food Chemistry*, 2016, 201,
616 37-45, DOI: 10.1016/j.foodchem.2016.01.012.
- 617 63. M. Yin, Z. Fu, X. Yu, X. Wang and Y. Lu, *Polymers*, 2025, 17, DOI:
618 10.3390/polym17121686.
- 619 64. V. Núñez Gómez, M. Jesús Periago, J. Luis Ordóñez Díaz, G. Pereira Caro, J. Manuel
620 Moreno Rojas and R. González Barrio, *Food Research International*, 2024, 177, DOI:
621 10.1016/j.foodres.2023.113718.
- 622 65. S. Wanlapa, K. Wachirasiri, D. Sithisam-ang and T. Suwannatup, *International Journal of*
623 *Food Properties*, 2011, 18, 1306-1316, DOI: 10.1080/10942912.2010.535187.
- 624 66. C. Fu, D. Zhan, G. Tian, A. Yu, L. Yao and Z. Guo, *ACS Applied Materials & Interfaces*,
625 2024, 16, 35740-35751, DOI: 10.1021/acsami.4c05041.
- 626 67. M. Vera-Mahecha, M. A. Noriega and D. A. Castellanos, *Journal of Food Engineering*,
627 2025, 397, DOI: 10.1016/j.jfoodeng.2025.112605.
- 628 68. U. Michael Igolima, S. J. Abbey, A. O. Ifelebuegu and E. U. Eyo, *Materials*, 2023, 16,
629 DOI: 10.3390/ma16031092.
- 630 69. Q. Zhou, X. Jiang, Y. Guo, G. Zhang and W. Jiang, *Chemosphere*, 2018, 201, 519-529,
631 DOI: 10.1016/j.chemosphere.2018.03.045.
- 632 70. S. Zhao, Y. Li, M. Wang, B. Chen, Y. Zhang, Y. Sun, K. Chen, Q. Du, X. Pi, Y. Wang,
633 Z. Jing and Y. Jin, *International Journal of Biological Macromolecules*, 2023, 253, DOI:
634 10.1016/j.ijbiomac.2023.126458.
- 635 71. B. H. Hameed, *Journal of Hazardous Materials*, 2009, 162, 939-944, DOI:
636 10.1016/j.jhazmat.2008.05.120.
- 637 72. J. B. Adeoye, S. Y. Lau, Y. H. Tan, Y. Y. Tan, T. Chiong, N. M. Mubarak, G.
638 Anbucheziyan, M. Khalid and J. T. W. Ng, *Discover Applied Sciences*, 2025, 7, DOI:
639 10.1007/s42452-025-07250-4.
- 640 73. B. Qiu, Q. Shao, J. Shi, C. Yang and H. Chu, *Separation and Purification Technology*,
641 2022, 300, DOI: 10.1016/j.seppur.2022.121925.
- 642 74. W. Ji, H. Jin, H. Wang, S. Tabassum, Y. Lou, X. Fan, M. Ren and J. Wang, *Colloids and*
643 *Surfaces A: Physicochemical and Engineering Aspects*, 2025, 715, DOI:
644 10.1016/j.colsurfa.2025.136615.
- 645 75. S. R. Al Mhyawi, N. A. H. Abdel Tawab and R. M. El Nashar, *Polymers*, 2023, 15, DOI:
646 10.3390/polym15020277.
- 647 76. N. Khumalo, S. Mohomane, V. Elumalai and T. Motaung, *Polymers*, 2025, 17, DOI:
648 10.3390/polym17222983.
- 649 77. N. I. I. Zamri, S. L. N. Zulmajdi, N. Z. A. Daud, A. H. Mahadi, E. Kusrini and A. Usman,
650 *SN Applied Sciences*, 2021, 3, DOI: 10.1007/s42452-021-04245-9.
- 651 78. J. Qiu, P. Fan, Y. Feng, F. Liu, C. Ling and A. Li, *Environmental Pollution*, 2019, 254,
652 DOI: 10.1016/j.envpol.2019.113117.



653

654

Open Access Article. Published on 21 April 2026. Downloaded on 4/21/2026 8:39:03 PM.

This article is licensed under a Creative Commons Attribution-NonCommercial 3.0 Unported Licence.



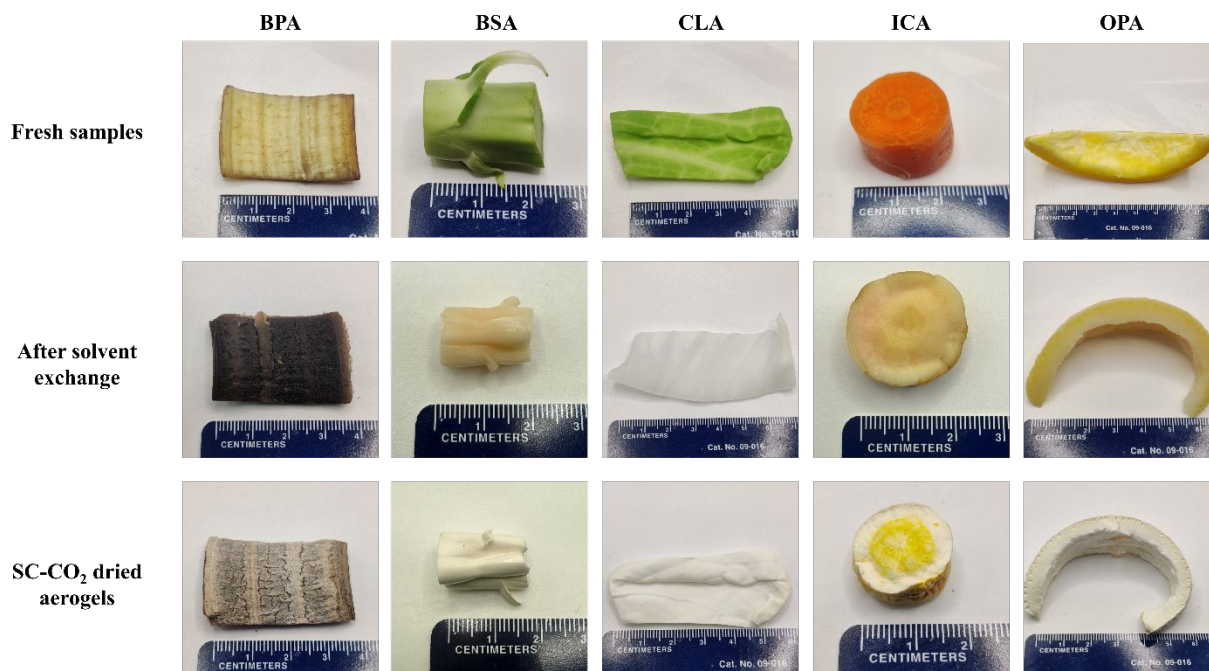
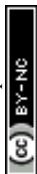
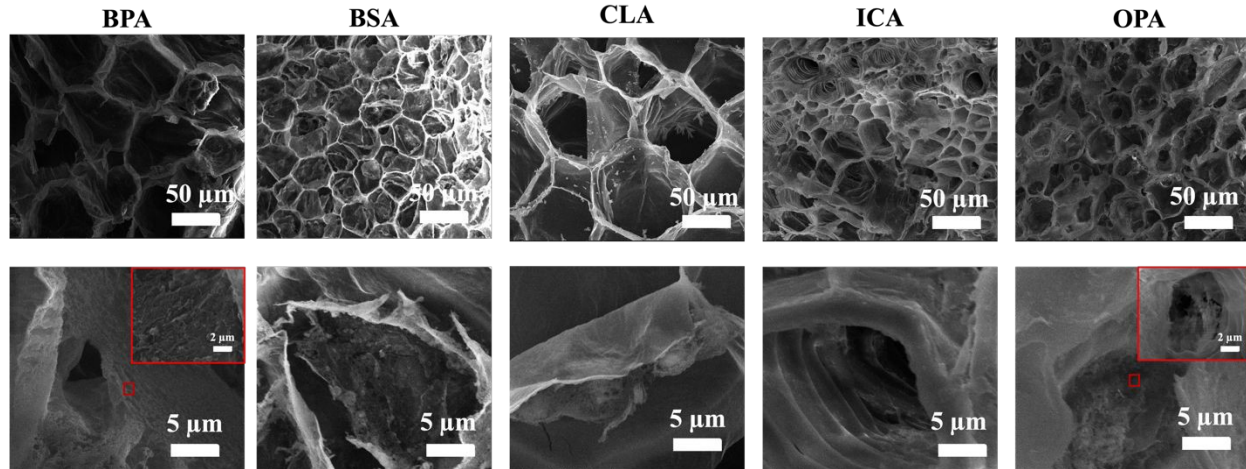


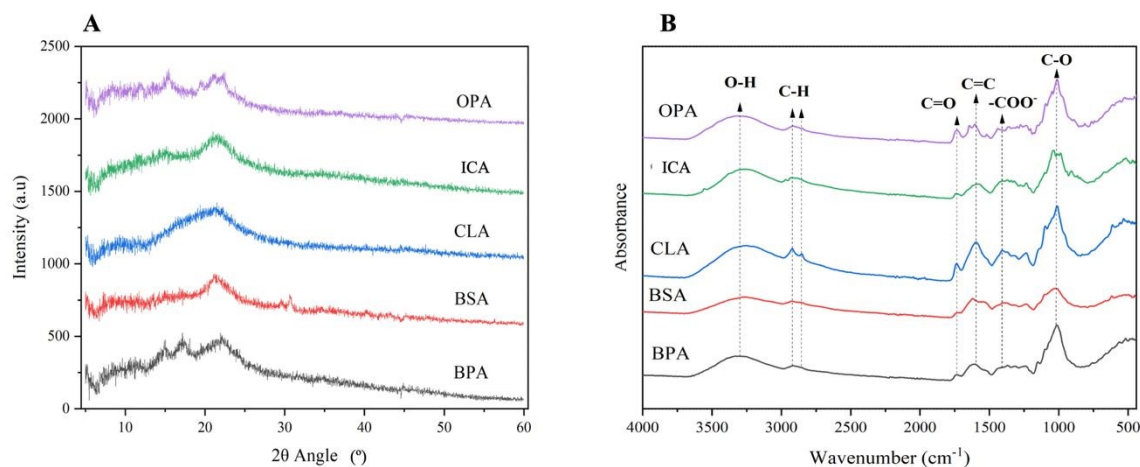
Fig. 1. Photographs of the aerogel at different stages of processing: fresh, solvent exchange, and dried stages. BPA: Banana peel aerogel; BSA: Broccoli stem aerogel; CLA: Cabbage leaf aerogel; ICA: Imperfect carrot aerogel, and OPA: orange peel aerogel.





660
661 **Fig. 2.** SEM images of fruits and vegetable waste aerogels taken at 500 × and 5000 ×. BPA:
662 Banana peel aerogel; BSA: Broccoli stem aerogel; CLA: Cabbage leaf aerogel; ICA: Imperfect
663 carrot aerogel, and OPA: Orange peel aerogel.





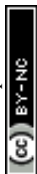
668

669 **Fig. 3.** The a) XRD patterns and b) FTIR spectrum of fruits and vegetable waste aerogels. BPA:

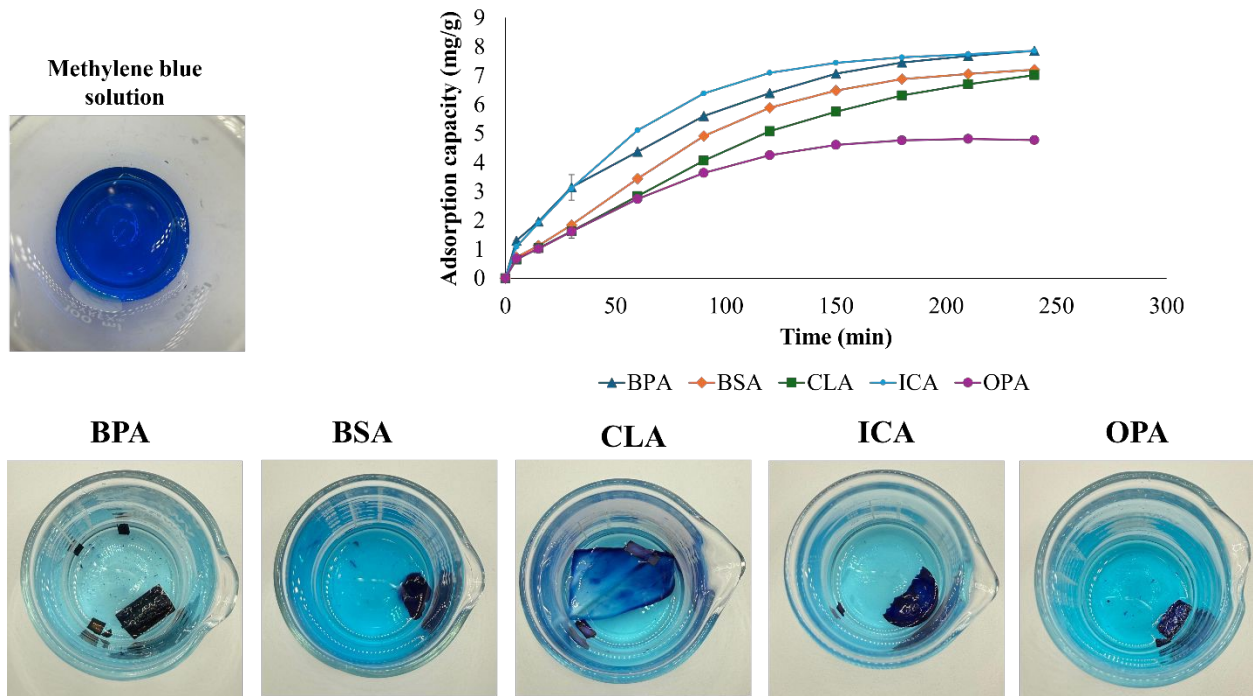
670 Banana peel aerogel; BSA: Broccoli stem aerogel; CLA: Cabbage leaf aerogel; ICA: Imperfect

671 carrot aerogel, and OPA: Orange peel aerogel.

672



673



674

675 **Fig. 4.** Methylene blue adsorption capacity of aerogels. BPA: Banana peel aerogel; BSA:

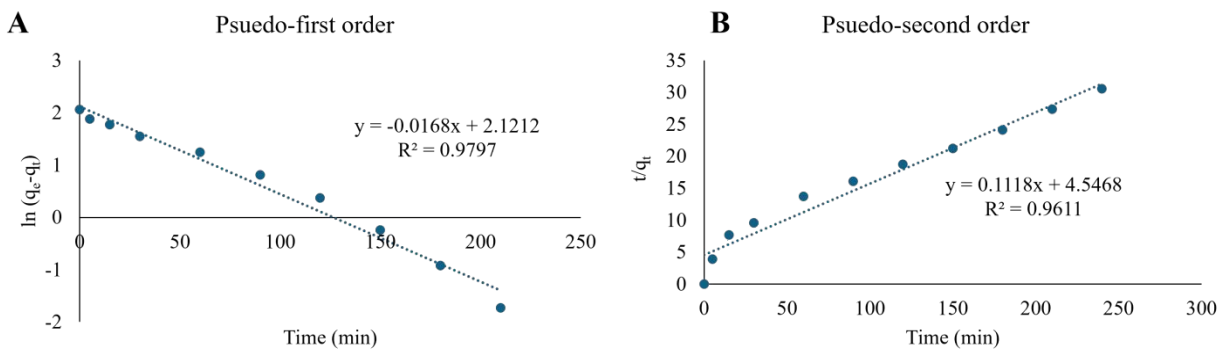
676 Broccoli stem aerogel; CLA: Cabbage leaf aerogel; ICA: Imperfect carrot aerogel, and OPA:

677 Orange peel aerogel.

678

679



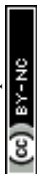


680

681 **Fig. 5.** Adsorption kinetics of methylene blue adsorption for a) pseudo-first order model and b)

682 pseudo-second order model for BPA (Banana peel aerogel).

683



Data availability statement

The data supporting this article have been included as part of the current article.

